



Research article

Switching from weak to strong cortical attachment of microtubules accounts for the transition from nuclear centration to spindle elongation in metazoans

Shohei Tada^a, Yoshitaka Yamazaki^a, Kazunori Yamamoto^{b,c,d,e}, Ken Fujii^{b,c}, Takahiro G. Yamada^{a,f}, Noriko F. Hiroi^{g,h}, Akatsuki Kimura^{b,c,i,*}, Akira Funahashi^{a,f,*}

^a Center for Biosciences and Informatics, Graduate School of Fundamental Science and Technology, Keio University, Yokohama, Kanagawa, 223-8522, Japan

^b Cell Architecture Laboratory, Department of Chromosome Science, National Institute of Genetics, Mishima, Shizuoka 411-8540, Japan

^c Genetics Program, The Graduate University for Advanced Studies, SOKENDAI, Mishima, Shizuoka 411-8540, Japan

^d Faculty of Applied Bioscience, Kanagawa Institute of Technology, Atsugi, Kanagawa, 243-0292, Japan

^e Division of Developmental Physiology, Institute for Genetic Medicine, Hokkaido University, Sapporo, Hokkaido, 060-0815, Japan

^f Department of Biosciences and Informatics, Keio University, Yokohama, Kanagawa, 223-8522, Japan

^g School of Medicine, Keio University, Shinjuku-ward, Tokyo, 160-8582, Japan

^h Faculty of Creative Engineering, Kanagawa Institute of Technology, Atsugi, Kanagawa, 243-0292, Japan

ⁱ Center for Data Assimilation Research and Applications, Joint Support-Center for Data Science Research, Research Organization of Information and Systems (ROIS), Tachikawa, 190-8562, Japan

ARTICLE INFO

Dataset link: <https://github.com/funabio/MTSim>

Keywords:

Cell cycle
Mathematical modeling
Astral microtubules
Centrosome centration
Spindle elongation

ABSTRACT

The centrosome is a major microtubule organizing center in animal cells. The position of the centrosomes inside the cell is important for cell functions such as cell cycle, and thus should be tightly regulated. Theoretical models based on the forces generated along the microtubules have been proposed to account for the dynamic movements of the centrosomes during the cell cycle. These models, however, often adopted inconsistent assumptions to explain distinct but successive movements, thus preventing a unified model for centrosome positioning. For the centration of the centrosomes, weak attachment of the astral microtubules to the cell cortex was assumed. In contrast, for the separation of the centrosomes during spindle elongation, strong attachment was assumed. Here, we mathematically analyzed these processes at steady state and found that the different assumptions are proper for each process. We experimentally validated our conclusion using nematode and sea urchin embryos by manipulating their shapes. Our results suggest the existence of a molecular mechanism that converts the cortical attachment from weak to strong during the transition from centrosome centration to spindle elongation.

1. Introduction

Cell cycle is a vital and dynamic phenomenon for all living organisms, during which the cell itself and its components change their shapes and positions. Physical forces generated through the activities of macromolecules play central roles in these dynamics [1,2].

* Corresponding authors.

E-mail addresses: akkimura@nig.ac.jp (A. Kimura), funa@bio.keio.ac.jp (A. Funahashi).

<https://doi.org/10.1016/j.heliyon.2024.e25494>

Received 20 August 2023; Received in revised form 6 January 2024; Accepted 29 January 2024

Available online 5 February 2024

2405-8440/© 2024 The Authors. Published by Elsevier Ltd. This is an open access article under the CC BY-NC-ND license (<http://creativecommons.org/licenses/by-nc-nd/4.0/>).

In addition to uncovering the molecules involved in the processes, many researchers have attempted to understand the mechanisms of cell cycle by using dynamic models based on mechanical forces.

The positioning of the centrosomes is one of the key processes to define the spatial dynamics of animal cells during cell cycle [3]. In the case of newly fertilized embryos, the centrosomes first move with sperm- and oocyte-derived pronuclei to the cell center [4,5]. After the formation of the mitotic spindle, the centrosomes, which act as the two poles of the spindle, move toward the two poles of the cell to elongate the spindle and separate the chromosomes into the daughter cells. The process of spindle elongation occasionally takes place simultaneously with the displacement of the spindle from the cell center, for example in the nematode embryo, which results in asymmetric cell division [6]. Major key forces driving the correct positioning of the centrosomes are generated along microtubules, which are nucleated from the centrosomes and grow and shrink dynamically in the cell [7]. A number of proteins have been identified that regulate the microtubule-based forces (for example [8–10]), and the mechanisms underlying force generation and centrosome movements have been revealed [11,12].

These molecular and mechanical analyses of centrosome positioning produced the data to create numerical simulations to explain the observed phenomenon. Previous studies proposed a simulation model based on cytoplasmic pulling forces on microtubules [3,5,13,14] during the movement of the centrosome, together with the nucleus, toward the cell center [15–18]. These models agree quantitatively with the actual movements of the centrosomes in the one-cell-stage embryos of the nematode *Caenorhabditis elegans* [15] and of sea urchins [18]. The precise mechanism for the force generation (i.e., whether the force is generated at the cortex or in the cytoplasm, the microtubules mediate pulling or pushing forces) is still under debate and may differ among the species [19–21]. In principle, however, for the microtubule-dependent centration process, the forces should be dependent on the length of the microtubules, with a larger pulling force or smaller pushing force for longer microtubules. In this study, we focused on length-dependent pulling forces, but our conclusion should not depend on the precise mechanism of microtubule-dependent force generation.

Another process we focused on in this study is the elongation of the mitotic spindle. After the centrosomes bring the nucleus to the cell center and the mitotic spindle is formed at the center, the centrosomes move toward the cell periphery to elongate the spindle and separate the sister chromatids. The process is also well studied in the *C. elegans* embryo. We have constructed a numerical model for the process previously [22]. Forces pulling the microtubules at the cortex are thought to play major roles in spindle elongation, and $G\alpha$ and related proteins at the cell cortex are required [9–11]. Our previous model agreed well with the extent and speed of spindle elongation, which correlated with the cell size, of both wild-type and $G\alpha$ -knockdown *C. elegans* embryos [22]. In the model, we assumed that microtubules are attached to the cell cortex strongly, so that the angles between the cortex and the microtubules, and the angle between the neighboring microtubules around the centrosomes, change dynamically.

These studies were informative to separately understand the dynamic behaviors of nuclear centration and spindle elongation. Placing these successive processes in a unified framework, however, is difficult because these models assumed different attachment strengths of the microtubules with the cell cortex and thus different angle configurations of the microtubules (Fig. 1). The model for nuclear centration assumed a weak attachment of microtubules to the cell cortex, and thus the angles between the neighboring microtubules around the centrosomes were fixed (Fig. 1A, [15,18]). We name this configuration of the microtubule (MT) as ‘MT-Fixed’. MT-Fixed configuration, in which the microtubules elongate from the centrosome with a uniform angle distribution at the initial configuration and these angles are fixed during the centrosome centration, seems natural unless there is a specific mechanism to bias the angle. In contrast, the model for spindle elongation assumed a strong attachment of microtubules to the cortex, and thus the angles were flexible (Fig. 1B, [22]). We name this configuration ‘MT-Variable’. The strong attachment of microtubules to the cortex during the spindle elongation in the *C. elegans* embryo is supported by the observation of Kozlowski et al. Cell (2007). Because multiple microtubules form a bundle, even if a single microtubule is dynamically attaching and detaching with the cortex, some of the microtubules in the bundle remain attaching to the cortex. In this way, the contact point of the MT bundle can be maintained. Live cell imaging of microtubules in embryos appears consistent with the differences in the attachment strength at each stage and angular configuration of microtubules [15,23]. The observation implies that the dynamics of the microtubules is switching between these two processes. However, the details remain unclear.

In this study, we examined the switching between these two processes during centrosome centration and spindle elongation, which account for the movement of the centrosome-nucleus complex and elongated pole-to-pole distance. To do so, we compared simulation results of models in which the angular configuration of microtubules (MTs) changes dynamically (MT-Variable model) or is fixed (MT-Fixed model). Using theoretical analyses and experimental measurements in nematode (*C. elegans*) and sea urchin (*Scaphechinus mirabilis*), we showed that MT-Variable does not account for centration and MT-Fixed does not account for spindle elongation.

2. Results

2.1. The MT-Fixed—but not the MT-Variable—configuration accounts for centrosome centration

In the previous studies, the “MT-Fixed” was assumed for centrosome centration [15,24,17]. In contrast, whether the “MT-Variable” could account for centrosome centration had never been examined. We ran simulations with both the MT-Fixed and MT-Variable assumptions by using microtubules that stochastically elongate and shrink, as done before for the *C. elegans* embryo [15,17,24].

In *C. elegans* embryos, in addition to the center-directed translational movement of the centrosome-nucleus complex, the axis connecting two centrosomes rotates from perpendicular to parallel to the major axis [12,24]. The MT Fixed assumption has reproduced

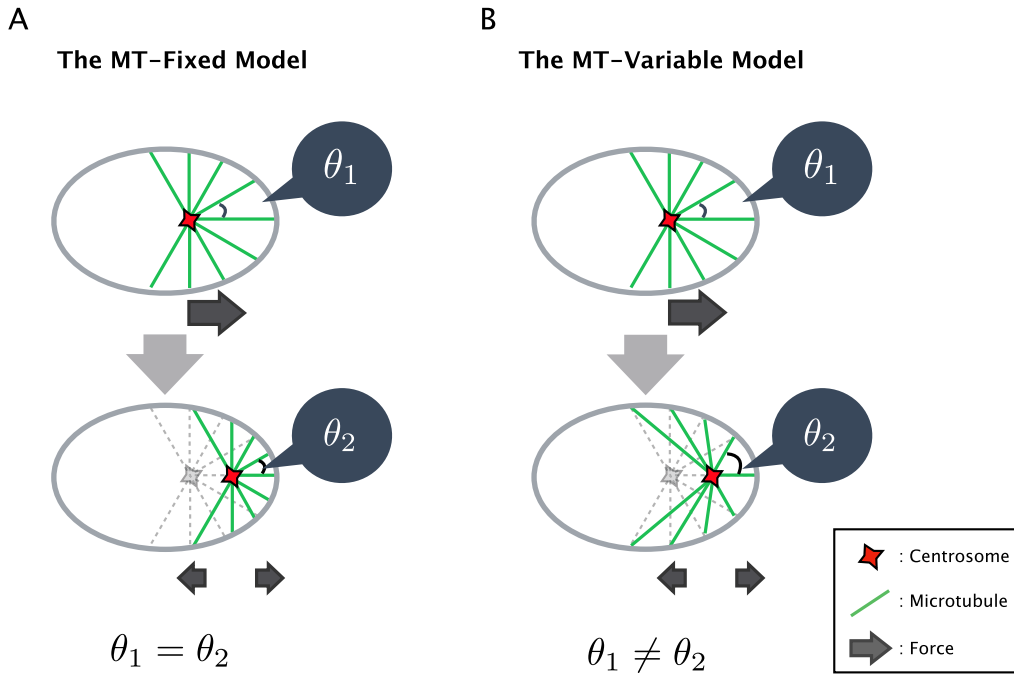


Fig. 1. Schema of the configuration of microtubules during spindle elongation in the MT-Fixed and the MT-Variable models. A: The schematic view of the model assuming MT-Fixed. The angle configuration of microtubules is fixed regardless of centrosome migration. B: The schematic view of the model assuming MT-Variable. The configuration of microtubules is changed by centrosome migration, because the ends of the microtubules are fixed on the cell cortex. Also, in spindle elongation, the two centrosomes are controlled independently.

Table 1
Parameter values in centrosome centration.

	Standard state	Range	Measured value	Ref.
Cell size (long axis) [$\times 10^{-6}$ m]	25			
Cell size (short axis) [$\times 10^{-6}$ m]	15			
Radius of nucleus-centrosome complex [$\times 10^{-6}$ m]	5			
Microtubules				
Growing velocity (V_g) [$\times 10^{-6}$ m/s]	0.25	0.118 - 0.328	0.118 - 0.328	*
Shrinking velocity (V_s) [$\times 10^{-6}$ m/s]	0.3	0.157 - 0.537	0.157 - 0.537	*
Catastrophe frequency (f_{car}) [1/s]	0.02	0.0115 - 0.046	0.0115 - 0.046	*
Rescue frequency (f_{res}) [1/s]	0.07	0.0113 - 0.133	0.0113 - 0.133	*
The number of microtubules (N)	208	30 - 550	>30	[15]
Motor protein				
Length-dependent pulling model				
Pulling force (F_{static}) [$\times 10^{-12}$ N]	1.1	0.5 - 1.5	0.78 - 1.1	**
Maximum velocity (V_{max}) [$\times 10^{-6}$ m/s]	2.0	0.5 - 5.0	1.1 - 2.0	[53,54]
Density on microtubule (D) [$\times 10^3$ /m]	100	20 - 500		
Drag of nucleus (fluid resistance)				
Viscosity of cytosol (η) [Ns/m ²]	1	0.001-10	0.0018-3	[46]
Stoke's radius (r) [$\times 10^{-6}$ m]	10	5-15	5-15	
Time step [s]	0.05	0.01-0.1		[55]

* [56–59]

** [60,53,61]

this rotational movement [24]. We used these observed results to compare two assumptions, focusing on the position of the nucleus-centrosome complex and the rotation angle of nucleus-centrosome complex from an initial state, ϕ (Fig. 2A). In the simulation, parameter values were set based on the previous studies [15,17,24] and are called the standard state in this study (Table 1).

First, we performed simulation of centrosome centration with MT-Fixed and MT-Variable model and evaluated the converged position of the nucleus-centrosome complex in the simulation of centrosome centration (Fig. 2B, Supplementary Movie S1 and S2). The nucleus-centrosome complex moved to the center, 50% of the cell size, in the MT-Fixed model, but moved only 25% of the cell size in the model with the MT-Variable assumption.

Next, we compared the rotation angle of the nucleus-centrosome complex (Fig. 2C). In the MT-Fixed model, the complex rotated, whereas in the MT-Variable model its rotation did not occur and the angle remained nearly 0°.

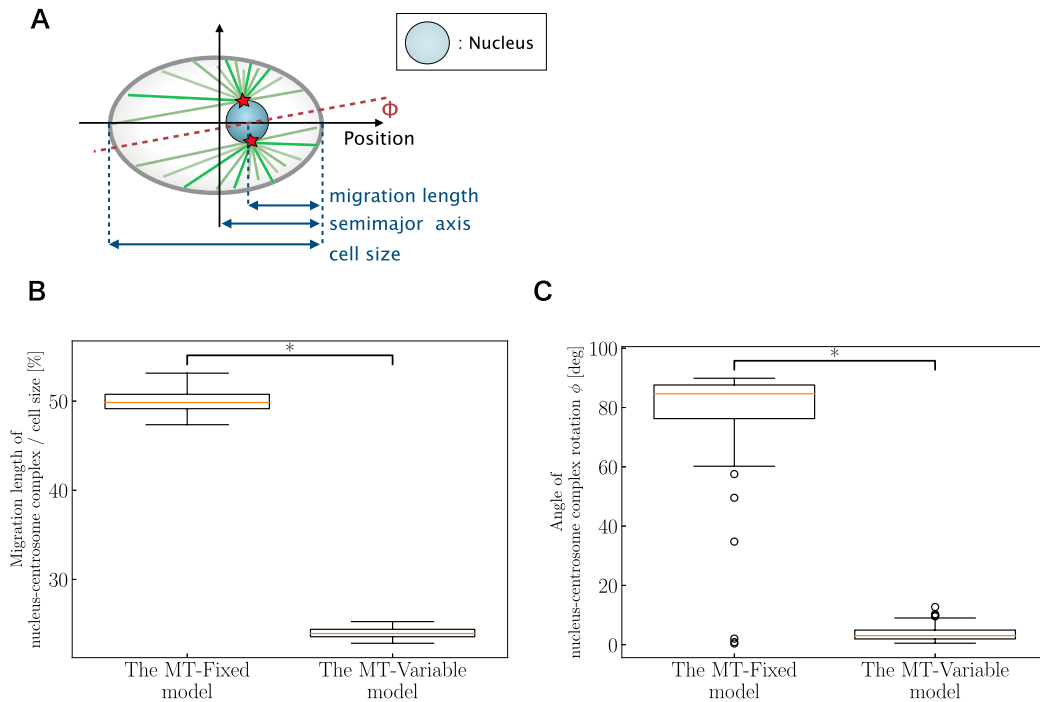


Fig. 2. The MT-Fixed—but not the MT-Variable—configuration accounts for centrosome centration. A: Schematic of centrosome centration. We defined migration length normalized to cell size as the position of the nucleus-centrosome complex and defined the angle of nucleus-centrosome complex rotation from an initial state as ϕ . B: Migration length normalized to cell size, 15 minutes after centrosome centration started ($n = 50$). There was a significant difference between the models (Wilcoxon rank-sum test $p < 2.2 \times 10^{-16}$). C: Angle of nucleus-centrosome complex rotation, 15 minutes after centrosome centration started ($n = 50$). There was a significant difference between the models (Wilcoxon rank-sum test, $p = 1.39 \times 10^{-14}$).

These results indicate that the MT-Variable assumption does not account for centrosome centration, and the MT-Fixed assumption is critical for centration.

2.2. Centrosome centration is achieved by the model assuming MT-Fixed regardless of any initial position, angle, or cell shape

The simulation result of the previous section showed that the nucleus-centrosome complex moved to the center of the cell and rotated approximately 90° in the model assuming MT-Fixed with a specific initial position and angle of the nucleus-centrosome complex. We next investigated the robustness of the converged position and angle of the nucleus-centrosome complex against its initial position and angle using phase-plane analysis (Fig. 3A) [25]. This result showed one stable fixed point (the point where all arrows are attracted) at the center of the cell and 90° of rotation and two unstable fixed points (the point where some arrows are attracted and others are repulsed) at the center and 0° and 180° of rotation angle. This indicated the model assuming MT-Fixed can explain the movement to the center of cells and the 90° rotational angle independent of the initial position and rotational angle of the nucleus-centrosome complex.

The previous studies demonstrated that nucleus-centrosome centration is consistently achieved in sea urchins even though the cell shape varies in terms of the aspect ratio [13,18], the ratio of the short axis length to the long axis length of the cell, which represents the degree of roundness. To verify this robustness, we performed phase-plane analyses for cells with various aspect ratios (Fig. 3B, C). Cells that were either ellipsoidal or spherical in shape, i.e., aspect ratios larger or smaller than that of the standard state, showed one stable and two unstable fixed points—entirely the same as the result from the standard state (Fig. 3B, green, red). The result of phase-plane analysis for spherical cells showed that the center of cells was always stable (Fig. 3C), but the dynamic rotation of the nucleus-centrosome was prevented based on the MT-Fixed assumption. We also tested whether the rotation of the centrosome in these spherical cells could be reproduced by the MT Variable model (Fig. S1). The results showed that the MT Variable model did not induce any change from the initial angle (Fig. S1A), and also showed only an inadequate shift to the center with respect to the convergence position (Fig. S1B).

2.3. Quantification of MT distribution during spindle elongation suggested that the competition for the cortical force generator between the two spindle poles is not critical for spindle elongation

After the achievement of correct nucleus-centrosome centration, the cell cycle proceeds to enter the process of spindle elongation. Our previous model of spindle elongation in the *C. elegans* embryo assumed the MT-Variable configuration [22] and accounted for the converged length of the elongated spindle and its cell-size dependency observed experimentally *in vivo* [22]. In the current study,

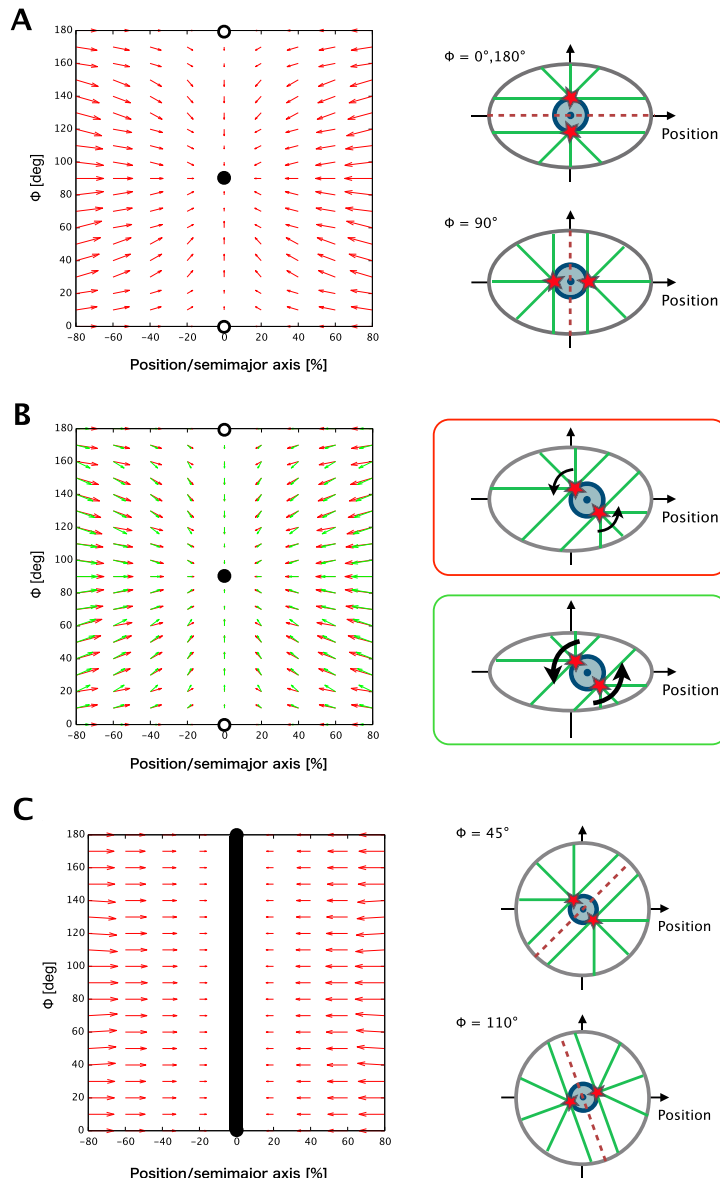


Fig. 3. Centrosome centration is achieved by the model assuming MT-Fixed regardless of any initial position, angle, or cell shape. A: Vector field about the movement of the nucleus-centrosome complex plotted against its position and angle. On the horizontal line, we used position normalized to the major axis. The vector field has a stable fixed point at the center and angle 90° , and two saddle points at the center and angles 0° and 180° . The standard states (Table 1) were used as parameter values in this simulation. B: More ellipsoidal shape (green: the length of minor axis = 10×10^{-6} m) produced more torque (vertical length of arrows) and rotation than the standard state (red). C: In spheres (major axis = 25×10^{-6} m, minor axis = 25×10^{-6} m), the cell center was stable regardless of angle.

we asked whether the MT-Fixed configuration could also account for the spindle elongation process. If so, switching from MT-Fixed at the centrosome centration to MT-Variable at spindle elongation would not be necessary.

Before comparing the MT-Variable and MT-Fixed models for spindle elongation, we evaluated the feasibility of the ‘‘Stoichiometric model’’, another model proposed for spindle elongation [26]. The critical mechanism for the spindle elongation in the stoichiometric model is the competition between the two centrosomes for the cortical force generators [26]. If each of the cortical force generator pulls only the nearest centrosome, the anterior centrosome is pulled selectively by the anterior cortical force generators and thus moves to the anterior direction until it reaches to the center of the anterior half of the cell, and vice versa. This model explains well experimental observations, such as the elongation independence of the initial length of the spindle [26]. Notably, the limited number of cortical force generators has been proposed as a potential mechanism to explain the centration of the centrosomes [27,28]. Therefore, the stoichiometric model is a potential model to explain both the centration and the spindle elongation.

We questioned whether the competition for the cortical force generators, which is critical for the stoichiometric model, really takes place during the spindle elongation in the *C. elegans* embryo. The MTs growing from the anterior centrosome toward the

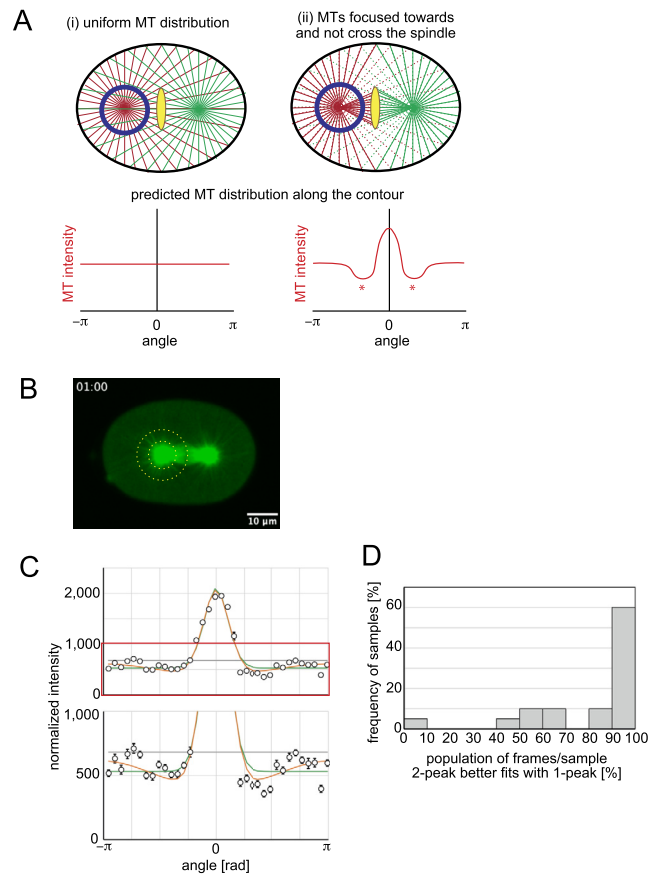


Fig. 4. MT distribution during the spindle elongation. A: Scheme of MT distribution in a uniform case (i, left) and in a case where MTs are focused toward the spindle and do not grow over the mitotic chromosomes (ii, right). Red and green lines indicate MTs from the left and right centrosome, respectively. Yellow indicates the mitotic chromosomes. In the case of (ii), there will be MT-sparse regions next to the MT-dense region because the MTs are focused toward the chromosomes, and also because the MTs from the farther centrosome do not elongate across the chromosomes. The dotted lines in (ii) indicate expected MTs of the uniform distribution. This will be reflected as the two valleys next to the largest peak when we quantify the MT intensity along a circumference whose center is one of the centrosome (blue circles) as drawn in the lower panels. In the lower panels, the angle of 0 is toward the other centrosome. B: A representative example of the β -tubulin::GFP image of the *C. elegans* embryo (AZ244 strain) during spindle elongation. See Supplemental Movie S3 for other frames of this embryo. C: A representative plot of the MT intensity within each angle window for 15 to 20 pixel length from the center of the left centrosome in (B). Red circles and bars represent mean and S.E.M. of the intensity of the angle window. Yellow, orange, and purple lines show the best fit lines with uniform, single peak von Mises, and double peak von Mises distribution, respectively. D: Distribution with respect to the number of frames for a better fit to a two-peak distribution for a frame-by-frame one-peak distribution in each sample.

posterior direction appears not to reach the posterior cortex (Fig. 4A(i)), but to be used as spindle MTs to capture the chromosomes and not reach to the posterior cortex, and vice versa (Fig. 4A(ii), B). If this is the case, the competition is not taking place. The anterior centrosome can monopolize the anterior force generators without competition. However, it was difficult to demonstrate whether the MTs from the anterior pole grow beyond the chromosome to reach the posterior cortex, because the MTs from the anterior and posterior centrosomes cannot be distinguished. To overcome this difficulty, we examined the angle distribution of the MTs before they reach the chromosomes (Fig. 4B, Supplemental Movie S3). If the MTs involved in the formation of the spindle do not reach the cell cortex, there should be MT sparse regions at the both sides of the spindle due to the focusing of the MTs for the spindle from the nearer centrosome, and also due to the limited elongation over the chromosome from the farther centrosome (Fig. 4A(ii)). This was actually the case. When we quantify the signal intensity of the β -tubulin for every 10° of the distance 3 to 4 μm , we detected MT-sparse regions next to the MT-dense region (Fig. 4C). This feature was supported in a statistical manner that a fitting with a double-peak distribution was more likely than that with a single-peak distribution (Fig. 4D). The experimental observations demonstrated that the competition of the cortical force generators is minor and thus the stoichiometric model is not necessary to explain the spindle elongation (see also Discussion).

2.4. The experimentally obtained MT distribution was consistent with MT-Variable configuration during spindle elongation in the nematode *C. elegans* embryo

To directly evaluate whether the MTs are fixed or variable, we tried to quantify the angle of MTs during spindle elongation (Fig. 5A, B). This was difficult because the filamentous signals of β -tubulin::GFP were not reliable enough to quantify the change in the angle of single filament over time. Nevertheless, we could quantify the angle distribution as we did for Fig. 4 and found

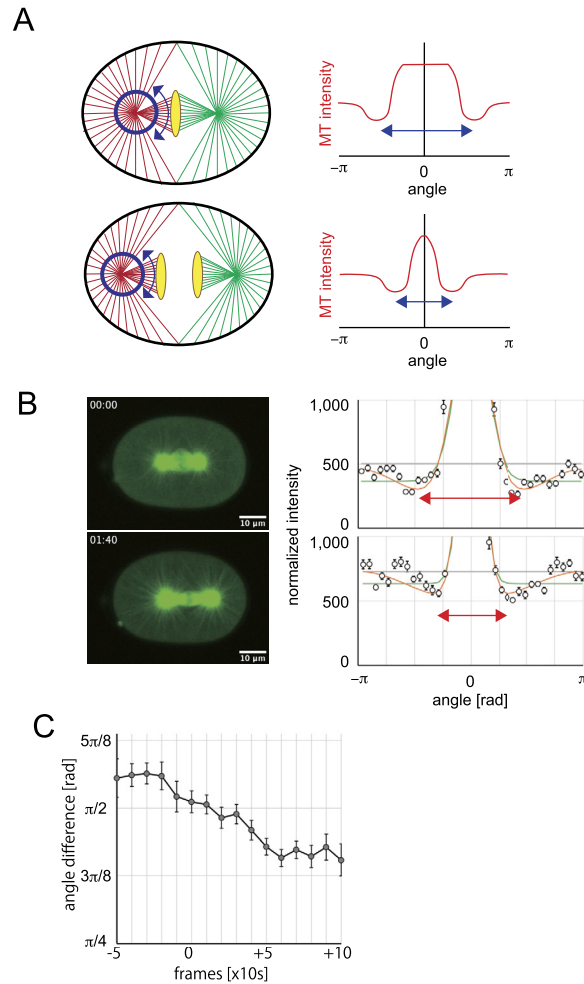


Fig. 5. MT distribution is consistent with MT-Variable model during the spindle elongation. A: Scheme of MT distribution for MT-Variable case. As the spindle elongates, the distance between the two valleys across the major peak (blue two-headed-arrows in left and right schematics) will decrease. The colors in the schema (left) are same as in Fig. 4A. B: Plots of the MT intensity at the initial time frame (frame 0) of the elongation and the final time frame (frame 13) before the onset of spindle rocking. The MT intensity was quantified using the β -tubulin::GFP expressing strain (AZ244). The major peaks became sharper, consistent with the MT-variable model. C: The change in angle for 6 centrosomes. The angle between the two valleys were plotted against time-frame normalized to the onset of the spindle elongation.

that the angle for the MT-sparse region decrease as the spindle elongates (Fig. 5B, C). This experimental observation supported the MT-variable model over MT-fixed model.

2.5. The MT-Fixed and the MT-Variable reproduced the converged length of the spindle after elongation and its cell-size dependency

To investigate which of the two configurations, MT-Fixed or MT-Variable, is more suitable for the spindle elongation from an independent approach, we constructed simulation models to compare the MT-Variable and MT-Fixed configurations for the spindle elongation based on our previous study (Fig. 1) [22]. For simplicity, in the current study, we considered only the force-generator-limited mechanism assumed for the $G\alpha$ -dependent force but not the mechanism for the $G\alpha$ -independent force, because the former plays the major role [22].

We performed simulation of spindle elongation with MT-Fixed and MT-Variable model and evaluated the converged position of centrosomes in the simulation of spindle elongation in cells of various sizes (Fig. S2, Supplementary Movie S4 and S5). Both the MT-Fixed and the MT-Variable configurations reproduced the converged length of the spindle after elongation and its cell-size dependency (Fig. S2) quantified in the previous experiments of the *C. elegans* embryo (Fig. S2, red line) [22]. Thus, the spindle length and its cell-size dependency are insufficient to distinguish between the validity of the MT-Fixed and MT-Variable configurations.

2.6. The MT-Fixed and MT-Variable configurations predict distinct aspect-ratio dependency of the spindle elongation

Next, we focused on the effect of cell shape on the length of spindle elongation, focusing on the aspect ratio as an index of cell shape. The models based on the MT-Fixed and MT-Variable configurations predicted distinct aspect-ratio dependency of the

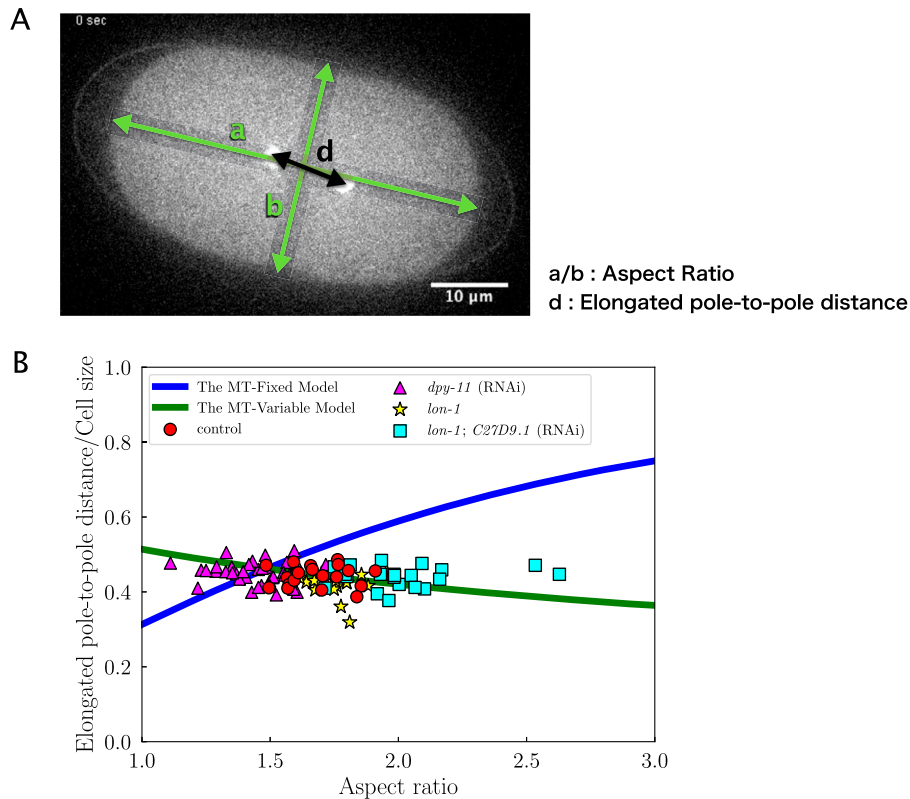


Fig. 6. The MT-Variable—but not the MT-Fixed—configuration accounts for the experimentally obtained aspect-ratio dependency of spindle elongation in the nematode *C. elegans*. A: Example of aspect ratio and elongated pole-to-pole distance measurements for *C. elegans* embryos. B: Blue and green lines show the simulation results of the MT-Fixed and MT-Variable models, respectively. The positions of the spindle poles were visualized using γ -tubulin::GFP expressing strains. Each point refers to a result measured experimentally for *C. elegans*. The distinct shapes of the points represent the distinct strains and gene knockdowns of *C. elegans*. Strains used are TH27, TH32 and CAL1628 (see Method).

converged length of the elongated spindle (Fig. 6). In the MT-Fixed model, the elongation length increased gradually as the aspect ratio increased (Fig. 6, blue line). In contrast, in the MT-Variable model, the elongation length slightly decreased as the aspect ratio increased (Fig. 6, green line).

2.7. The MT-Variable—but not MT-Fixed—configuration accounts for the experimentally obtained aspect-ratio dependency of spindle elongation in the nematode *C. elegans* embryo

To investigate which of the two configurations, MT-Fixed or MT Variable, is more suitable for the spindle elongation process, we experimentally measured the aspect-ratio dependency of the spindle elongation in the *C. elegans* embryo. We decreased the aspect ratio of *C. elegans* embryos by knocking down the *dpy-11* gene or increased it by knocking down the *C27D9.1* gene in a *lon-1* mutant [29]. We visualized the centrosomes using strains expressing γ -tubulin fused to green fluorescent protein (GFP) (Fig. S3) and measured the converged length of the elongated spindles (Fig. 6A). The experimental data aligned along the line predicted by the MT-Variable—but not the MT-Fixed—model, supporting the involvement of the MT-Variable configuration for the spindle elongation process (Fig. 6B).

Our present models contained parameters whose values were not clear in the previous research, such as the initial angle and the density of the microtubules. To evaluate the effect of their uncertainty, we conducted simulations in which the values of these parameters were widely changed (Figs. S4, S5). These parameters did not affect the trends of the aspect-ratio dependency of the spindle elongation, further supporting MT-Variable for spindle elongation. Interestingly, this analysis also revealed that the elongation length did not change markedly when we changed the values of the parameters in the MT-Variable configuration, indicating that the MT-Variable configuration enables more robust elongation than the MT-Fixed configuration.

2.8. The MT-Variable configuration also accounts for the aspect-ratio dependency of spindle elongation in the sea urchin embryo

We conducted similar experiments in the sea urchin *S. mirabilis*. The manipulation of the aspect ratio for *S. mirabilis* was realized by embedding the fertilized eggs into a fabricated microdevice containing cylinders with various aspect ratios (Fig. S6), as developed previously [13]. During the spindle elongation in *S. mirabilis*, microtubules reached the cell cortex, and astral microtubules

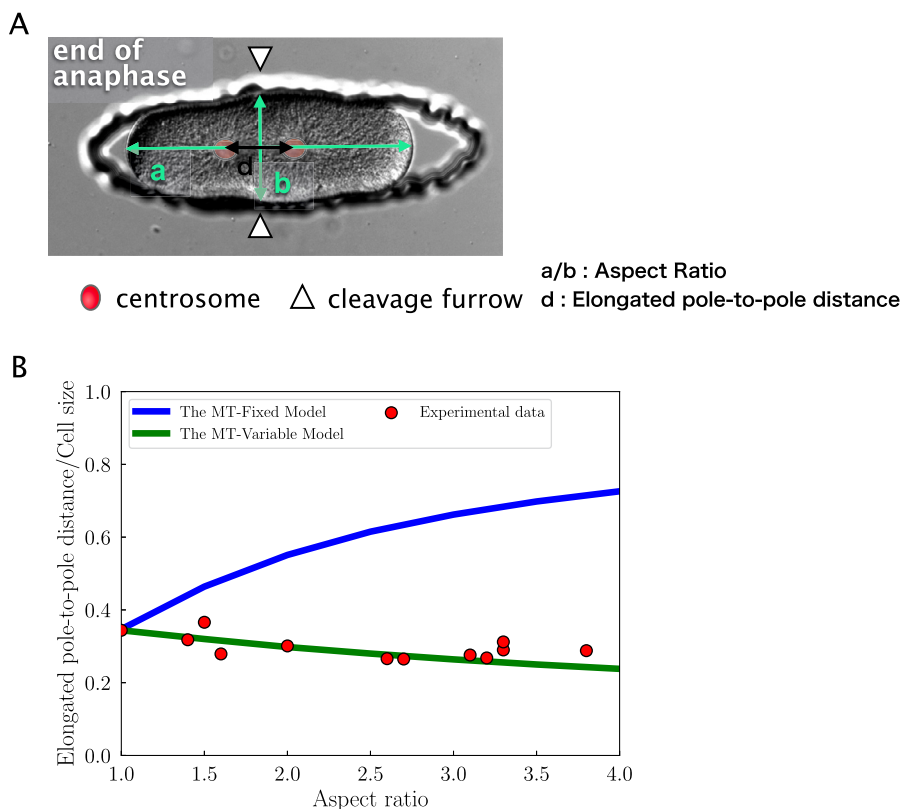


Fig. 7. The MT-Variable—but not MT-Fixed—configuration accounts for the experimentally obtained aspect-ratio dependency of spindle elongation in the sea urchin *S. mirabilis*. A: Example of aspect ratio and elongated pole-to-pole distance measurements for *S. mirabilis* embryos. B: Blue and green lines show the simulation results of the MT-Fixed and MT-Variable model, respectively. The points refer to the results measured experimentally for *S. mirabilis*.

appeared dominant over inter-polar microtubules [30,31], suggesting the importance of cortical pulling forces. The converged length of the elongated spindle was measured from Nomarski DIC microscope images (Fig. 7A). The aspect-ratio dependency of the spindle elongation in *S. mirabilis* also agreed with the prediction from the MT-Variable model, indicating generalizability of the MT-Variable configuration during spindle elongation in metazoans (Fig. 7B).

3. Discussion

3.1. The angle configuration of microtubules in centrosome centration and spindle elongation

Previous research assumed the MT-Fixed configuration for the centration of the nucleus-centrosome complex, whereas the MT-Variable configuration was assumed for spindle elongation [15,22]. The current study investigated whether the different assumptions for the successive processes were appropriate, or whether one of the two configurations could account for both processes. We conducted simulations with both models, for both centrosome centration and spindle elongation. By comparing the model prediction with the experimental measurements, we clarified that the MT-Variable does not account for centrosome centration, and the MT-Fixed does not account for spindle elongation (Figs. 2, 3, 6B, 7B). The results support the idea that the cell switches from the MT-Fixed to the MT-Variable configuration upon the transition from centrosome centration to spindle elongation.

The dependency of the spindle elongation length on aspect ratio of the cell did not change much when we changed the values of the parameters in the MT-Variable configuration, indicating that the MT-Variable configuration enables more robust elongation than the MT-Fixed configuration. The main reason of the robustness based on this mechanical point of view is that the length of microtubules reaching the cortex from the spindle toward the long axis with the increase in aspect ratio is considered to be important. In the MT-Fixed model, the microtubule angles are fixed from beginning to end, so an increase in the aspect ratio directly leads to an increase in the length of the microtubules, which in turn leads to an increase in the forces that each microtubule pulled. This induces a strong pulling force on the spindle in the cortical direction, which is thought to lead to a large increase in the distance between spindles as the aspect ratio increases. In the case of MT-Variable, on the other hand, such an extreme increase in force can be tolerated by changing the angle of microtubules. In other words, by fixing the junction point between the microtubule and cortex, the angle of the microtubule changes with the movement of the spindle in a manner that reduces the long-axis component, thus allowing the change in aspect ratio to remain somewhat tolerant without producing the extreme change in elongated spindle distance seen in MT-Fixed. This is the reason why the aspect ratio of the spindles is somewhat tolerant to its change. Considering

the importance of cell division processes, including spindle elongation, using mechanisms that can withstand parameter fluctuations, such as the MT-Variable configuration, is preferable for robust spindle elongation. We also quantified the difference between the initial angle and the angle at convergence of each microtubule based on simulation results for *C. elegans* and *S. mirabilis* in order to verify how much of this angular change actually occurs is sufficient for the achievement of spindle elongation (Fig. S7). As a result, we observed a change in angle of approximately 20 degrees, independent of the species, as well as the aspect ratio. This result suggests that a large angular change is not required for spindle elongation to occur and that the change from microtubule angle fixation in centrosome centration is not so dramatic.

In previous studies, the force on microtubules has been formulated as proportional to the length of the microtubule or the square of the length of the microtubule, and has been extensively verified [3,27,13,16,19]. In this study, we assumed a force proportional to the length of the microtubule for centrosome centration and to its square for spindle elongation. Therefore, we replaced each of these assumed forces and verified the position of the centrosomes, its angle of rotation, and the pole-to-pole distance at the point of convergence (Fig. S8 and S9). As a result, there was no significant difference in the position of convergence in the centrosome centration and the distance between the poles in the spindle elongation for either force assumption (Figs. S8A and S9). On the other hand, a tendency for significantly slower rotation was confirmed by making the force proportional to the square of the microtubule length with respect to the angle of rotation in the centrosome centration (Fig. S8B). These results generally indicated that the mechanism that determines the convergence position is not the force generation mechanism but the angular distribution of the microtubules that we have shown in this study. The rotation of the centrosomes only moderates the speed based on the force proportional to the square of the microtubule length, indicating that the angular distribution of the microtubules is important in determining the state of convergence.

3.2. Possible mechanisms of the switch from the MT-Fixed to the MT-Variable configuration

We propose that the angle configuration of microtubules switches from MT-Fixed to MT-Variable when the cell transits from centrosome centration to spindle elongation. What is the mechanism underlying this switch? In MT-Variable, the interaction between the microtubules and the cell cortex should be strong to allow changing of the angles between the microtubules around the centrosomes. In contrast, in MT-Fixed, the interaction is weak, so that the cortical end of the microtubule can move, allowing the original angle around the centrosomes to remain unchanged. We speculate that the strength of the interaction between the microtubules and the cell cortex is controlled by two pathways. First, for the strong interaction, the microtubules should reach the cell cortex frequently. Second, the proteins involved in the interaction should be abundant at the cell cortex.

Concerning the first pathway, in anaphase, when the spindle elongates, astral microtubules are known to be longer than they are in the other phases, which allow the microtubules to reach to the cell cortex in *S. mirabilis* [30]. For the second pathway, the localization dynamics of dynein proteins is informative. Dynein is a protein complex working with the molecular motor dynein to pull the microtubules. Dynein associates with the G proteins GPR-1/2 and LIN-5 at the cell cortex. These proteins localize near the anterior pole during centrosome centration and gradually move to the cell cortex in the *C. elegans* embryo [32]. In MDCK cells (a canine cell line), dynein shows strong localization to the nuclear periphery at prophase and relocates to the cell cortex at anaphase [33]. These findings support that the interaction between the microtubule and the cell cortex can become stronger when spindle elongation occurs, and thus the microtubule configuration can switch from MT-Fixed to MT-Variable.

3.3. Some notes for the stoichiometric model

The stoichiometric model is a nice model to explain spindle elongation in the *C. elegans* embryo [26]. In the present study, we showed that the competition of the cortical force generators by the two centrosomes, which is the critical driving mechanism in the stoichiometric model, is unlikely to take place during the spindle elongation simply because the cortical regions covered by MT from each of the centrosome overlap little (Fig. 4). We did not deny the possibility of competition in cases where such overlap is evident. The stoichiometric model will thus be a good back-up mechanism to assure the proper spindle elongation even when the MT distribution is mis-regulated.

The stoichiometric model is reported have higher capability over the MT-variable model [22] to explain the spindle elongation [26]. Specifically, the final spindle length after elongation is sensitive to the initial spindle length in the MT-variable model, but not in the stoichiometric model. This dependency is not so evident in vivo supporting the stoichiometric model over MT-variable model [26]. The examined “independency” has not been examined in the wide range of the initial length and thus we do not think this is a strong evidence to deny the MT-variable model. Further investigations are required. It will be interesting to search for a new model unifying both MT-variable and stoichiometric model, rather than denying one of them. The stoichiometric model has a potential to explain both the centration and the spindle elongation as we discussed in the result section. Such investigation will lead to a unified model for the centrosome movement.

3.4. Applicability of the present models to other mechanisms and cell systems

For the centrosome centration, we adopted the cytoplasmic pulling forces as the underlying force generation mechanism. This mechanism assumes that the force is generated on the microtubule throughout the cytoplasm [5,15]. However, the mechanism for the force generation driving the centrosome centration is still under debate and may differ among species. The pulling force may be generated at the cortex but not at the cytoplasm. In addition, the centration may be driven not by pulling forces but by the

pushing forces generated when the microtubules grow against the cell cortex [19,20,34,35]. Regardless of the detailed mechanism, for microtubules to accomplish centration, longer microtubules must generate or mediate stronger pulling forces or weaker pushing forces. We expect that the conclusions of our modeling studies do not depend on the details of the force generation mechanisms.

Our model of spindle elongation assumes forces pulling the two centrosomes from the cell cortex via the astral microtubules. This assumption is consistent with previous models and experiments [36], including those from *C. elegans* [37] and sea urchins [30,31,38,39]. Another popular driving force for spindle elongation is kinesin motors in the spindle microtubules pushing the two centrosomes apart. In the embryo of *Drosophila melanogaster*, spindle elongation is completely suppressed by inhibition of kinesin-5 (KLP61F), which controls the movement of interpolar microtubules [36]. In contrast, in *C. elegans*, the kinesin ortholog is not required for spindle elongation [40]. Our modeling results for the spindle elongation may be limited to cell types or organisms where the pulling forces from the outside of the spindle are dominant. The universality of this ability to switch the angle configuration of microtubules needs the further investigation in other species whose spindle elongation is controlled by pushing forces mediated by interpolar microtubules.

4. Star + methods

4.1. Key resources table

REAGENT or RESOURCE	SOURCE	IDENTIFIER
Chemicals, peptides, and recombinant proteins		
Deposited data		
Raw and analyzed data	This paper	https://github.com/funalab/MTSim
Experimental models: Organisms/strains		
<i>C. elegans</i> : Strain AZ244 [<i>unc-119(ed3) III</i> ; <i>ruls57.1</i>], TH27 [<i>unc-119(ed3) III</i> ; <i>ddIs6 V.</i>], CAL1628 [<i>lon-1(e185) III</i> ; <i>ddIs6 V.</i>], TH32 [<i>unc-119(ed3);ruls32 III</i> ; <i>ddIs6 V.</i>]		
Software and algorithms		
ImageJ		
MATLAB		

5. Resource availability

5.1. Lead contact

Further information and any related requests should be directed to and will be fulfilled by the lead contact, Prof. Akira Funahashi (funa@bio.keio.ac.jp).

5.2. Materials availability

This study did not generate new unique reagents.

5.3. Data and code availability

- The datasets generated and/or analyzed during the current study are available in the github repository, <https://github.com/funalab/MTSim>.
- The custom analysis codes created in this study are freely available through github (<https://github.com/funalab/MTSim>).

6. Experimental model and subject details

6.1. *C. elegans* sample preparation

The *C. elegans* strains used in this study were AZ244 [*unc-119(ed3) III*; *ruls57.1*] TH27 [*unc-119(ed3) III*; *ddIs6 V.*], CAL1628 [*lon-1(e185) III*; *ddIs6 V.*], and TH32 [*unc-119(ed3)*; *ruls32 III*; *ddIs6 V.*]. *ruls57* contains *pie-1p::GFP::tubulin*, *ddIs6* contains *pie-1p::tbg-1::GFP* and *ruls32* contains *pie-1p::GFP::H2B*. CAL1628 was constructed in this study by crossing TH27 and CB185 [*lon-1(e185) III*]. TH27, TH32, and CB185 were provided by the *Caenorhabditis* Genetics Center. *C. elegans* strains were maintained using a standard procedure [41].

The aspect ratio of the eggshell was changed by knocking down *dpy-11* (to make the cell round) or by using a *lon-1* mutant with or without knocking down *C27D9.1* (to make the cell elongated), as established previously [29]. They generated spherical and elongated embryos with the aspect ratio of 1.5 ± 0.2 (mean \pm SD) for knockdown of *dpy-11* and 2.3 ± 0.3 for knockdown of *C27D9.1* against the *lon-1* mutant, respectively, compared to wild type (1.6 ± 0.1). The knockdown of *dpy-11* and *C27D9.1* was established as described previously [29,42] by feeding RNAi using the *C. elegans* RNAi library (Source BioScience, Nottingham, UK) [43].

6.2. *S. mirabilis* sample preparation

Gametes of *S. mirabilis* were collected by intracoelomic injection of 1 mM acetylcholine in artificial seawater. Sperm were collected dry from the aboral surface and kept in the refrigerator at 4 °C. Unfertilized eggs were shed into a large volume of artificial seawater, rinsed three times in fresh artificial seawater, and stored settled at 15 °C in an incubator until use.

S. mirabilis eggs were fertilized by the addition of sperm diluted around 1:10,000 in artificial seawater. After 30 seconds, a large volume of 1 M urea in artificial seawater was added to the watch glass. Fertilized eggs were collected in the center by gentle shaking and moved to a new plate containing Ca²⁺-free artificial seawater. To remove the jelly coat and fertilized membrane, fertilized eggs were pipetted several times. The eggs were rinsed twice in Ca²⁺-free artificial seawater and moved into artificial seawater on an agar-coated plate.

7. Method details

7.1. Mathematical modeling

7.1.1. Centrosome centration

In this study, centrosome centration was modeled based on a length-dependent pulling model [15]. In our simulation, cell boundaries were considered to be ellipsoids, the nucleus-centrosome complex was considered to be a sphere, and microtubules elongating from the centrosomes associated with the cell nucleus were considered to be straight rods reaching the cortex. Migration of the nucleus-centrosome complex is driven only by the pulling force of microtubules pulled by motor proteins. In this length-dependent pulling model, it is assumed that microtubules are pulled by a minus-end-directed motor protein that exists uniformly in the cytoplasm [3] and that the number of motor proteins attaching to the microtubules is proportional to its length. Thus, the pulling force of a microtubule is proportional to its length. The pulling force of each microtubule, F_{pull} , is

$$F_{\text{pull}} = D \cdot L \cdot F_{\text{motor}}$$

D is the density of motor proteins on the microtubule, L is the length of the microtubule, and F_{motor} is the force pulled by one motor protein. In this model, the effect of membranes on microtubules is considered as negligibly small. The migration of the nucleus-centrosome complex was disturbed by viscous force during migration. As in our previous study, inertial force is neglected because the Reynolds number is low, and viscous force is dominant inside the cell [15,44]. Because the viscous force is proportional to the velocity of an object, translational movement of the nucleus and centrosome is expressed by the following equation:

$$F_{\text{total}} = \Gamma V_{\text{trans}}$$

where F_{total} is the force from microtubules to the nucleus-centrosome complex, Γ is the viscosity constant, and V_{trans} is the velocity of nuclear translational movement. Because the nucleus was considered a sphere, the viscosity constant Γ is $6\pi r\eta$ by Stoke's Law. Thus, V_{trans} is

$$V_{\text{trans}} = \frac{F_{\text{total}}}{6\pi r\eta}$$

where r is the Stoke's radius and η is the viscosity of the cytoplasm.

Force by microtubules also rotates the nucleus-centrosome complex. As with translational movement, the complex is approximated as a sphere, and the rotational moment $\mathbf{T}_{\text{total}}$ is

$$\mathbf{T}_{\text{total}} = 8\pi r^3 \eta \mathbf{W}_{\text{rot}}$$

\mathbf{W}_{rot} is the vector of angular velocity. By summing the force of each microtubule, $\mathbf{T}_{\text{total}}$ is written as

$$\mathbf{T}_{\text{total}} = \sum F_i (\mathbf{r}_i \times \mathbf{u}_i)$$

F_i is force by microtubule, \mathbf{r}_i is the vector of direction from microtubule to nucleus or centrosome, and \mathbf{u}_i is the unit vector of microtubules.

In centrosome centration, parameter values were set based on those in a previous study (Table 1).

7.1.2. Spindle elongation

Our previous study proposed a $G\alpha$ -dependent force (force-generator-limited model) and a $G\alpha$ -independent force (constant-pulling model) for spindle elongation [22]. In particular, this study showed that the $G\alpha$ -dependent force is stronger than the independent force in terms of cell-size dependence, i.e., the effect size on the extent of elongated spindle length relative to cell size (mean = 0.069 for knockdown of $G\alpha$ subunit protein coding genes, 0.18 for wild type). Therefore, in the current study, we modeled spindle elongation based on the force-generator-limited model, given that this dominant $G\alpha$ -dependent force is sufficient for examining the effect of different angular distributions on spindle elongation. In our simulation, cell boundaries were considered to be ellipsoids, and microtubules elongating from the centrosomes were considered to be straight rods reaching the cortex. We considered that interpolar microtubules have no effect [22,45] because spindle elongation in the embryos of *C. elegans* is not inhibited by cutting interpolar microtubules during anaphase [37]. Centrosome migrations are driven only by the pulling force of microtubules provided by motor

Table 2
Parameter values in spindle elongation (*C. elegans*).

	Values		Ref.
Drag of centrosome (fluid resistance)			
Viscosity of cytosol (η) [Ns/m ²]	1		[46]
Stoke's radius (r) [$\times 10^{-6}$ m]	1.5		[47]
Microtubules			
Density of microtubules [$/90^\circ$]	6		[22]
	MT-Fixed	MT-Variable	
Initial angle of microtubules [$^\circ$]	126	97	
Force-generator-limited model			
	MT-Fixed	MT-Variable	
Pulling force constant [$\times 10^{-3}$ N/m ²]	2.5	0.9	

Table 3
Parameter values in spindle elongation in *S. mirabilis*.

	Values		Ref.
Cell size (aspect ratio 1.0) [$\times 10^{-6}$ m]	120		This study
Cell height [$\times 10^{-6}$ m]	65		This study
Metaphase spindle length [$\times 10^{-6}$ m]	25		This study
Drag of centrosome (fluid resistance)			
Viscosity of cytosol (η) [Ns/m ²]	1		[46]
Stoke's radius (r) [$\times 10^{-6}$ m]	10		[38]
Microtubules			
Density of microtubules [$/90^\circ$]	20		
	MT-Fixed	MT-Variable	
Initial angle of microtubules [$^\circ$]	138	123	
Force-generator-limited model			
	MT-Fixed	MT-Variable	
Pulling force constant [$\times 10^{-4}$ N/m ²]	3.7	1.5	

proteins [22]. In the force-generator-limited model, microtubules are assumed to be pulled by dynein anchored to the cortex, and the number of dyneins is limited [22]. This assumption means that the pulling force from microtubules is proportional to the area of the cell membrane, and that is proportional to the squared length of the microtubule. In this model, the effect of membranes on microtubules is considered to be negligibly small. Centrosomes are affected by viscous force during migration. The relationship between centrosomes and viscous force is the same as the relationship between the nucleus-centrosome complex and viscous force in centrosome centration [22].

In spindle elongation, the values of cytosol viscosity, Stoke's radius, and microtubule density were set based on those in previous studies [22,46,47]. However, there are no direct measurements for the values of the initial angle of microtubules and the pulling force constant. Therefore, these values were estimated by manual parameter fitting of the simulation results to previously extracted experimental results [22]. These parameters were called the standard state in this study (Tables 2, S1). Parameters related to spatial configuration of microtubules were density of microtubules and initial angle of microtubules. The density of microtubules was the number of microtubules existing in a two-dimensional region 90° from centrosomes. The initial angles of the microtubules were limited to the angles at which microtubules grow from the centrosome to the center of the cell. These parameters allowed microtubules to grow evenly in three dimensions. These parameters were manually fitted for each in the MT-Fixed and MT-Variable models to best match the elongated spindle length in P0 cells. For the simulation for *S. mirabilis*, the parameter values were determined based on direct measurements or previous studies (Table 3).

8. Quantification and statistical analysis

8.1. Image processing

For Figs. 4 and 5, the center coordinates of the centrosomes were quantified using the SpotTracker plugin of ImageJ/FIJI [48] (<http://bigwww.epfl.ch/sage/soft/spottracker/>). Fluorescent intensity of soluble β -tubulin was determined by the peak intensity of the cytoplasm. After subtracting the intensity of the soluble β -tubulin, the fluorescent intensity of β -tubulin, which should correspond to that from MTs, were extracted for the arc-shaped region of 15 to 20 pixels for every 10° . The mean and S.E.M. of the intensity in the region were calculated ('normalized intensity' in Figs. 4C and 5B). The resultant intensity-vs-angle plot was fitted either to a uniform distribution $f(\theta) = C$, a von Mises distribution with single peak $f(\theta) = \frac{1}{2\pi I_0(\kappa)} \exp\{\kappa \cos(\theta - \mu)\}$, or a von Mises distribution with two peaks at the opposite angle $f(\theta) = \frac{1}{2\pi I_0(\kappa)} [\exp\{\kappa_1 \cos(\theta - \mu)\} + \exp\{\kappa_2 \cos(\theta - \mu - \pi)\}]$. We also tested wrapped Cauchy distribution instead of von Mises distributions and obtained similar trends. The fitting was conducted with a maximum likelihood

method assuming the error is distributed with the normal distribution of $N(\text{mean}, S.E.M.^2)$. The feasibility of the models were evaluated using AIC (Akaike's Information Criterion) [49,50]. The analyses were conducted using MATLAB software using the optimization toolbox for the fitting.

For Figs. 6 and 7, *C. elegans* embryos were observed by using a fluorescence microscope, and *S. mirabilis* embryos were observed by using a differential interference microscope. First, the major axis of the embryos in each microscopic image were visually determined. Then, a minor axis was determined by drawing an axis perpendicular to the major axis and of maximum length to a cell boundary. Finally, spindle length and cell size were manually measured using line tools in Fiji [51].

8.2. *C. elegans* sample preparation

For imaging of the *C. elegans*, embryos were cut out from adult worms in 0.75× egg-salt buffer at 22 °C. For Figs. 4 and 5, fluorescence signals excited with a 488-nm laser were visualized using a spinning-disk confocal system (CSU-MP; Yokogawa, Tokyo, Japan) mounted on an inverted microscope (IX71; Olympus, Tokyo, Japan) equipped with a 40×, 1.25 N.A. objective (UPlanSAPO; Olympus) and a 2× intermediate magnification. For about 6 min, including the entire process of spindle elongation at the 1-cell-stage embryo, digital images were acquired every 10 s with an EM-CCD camera (iXon; Andor Technology, Belfast, UK) controlled by NIS elements software with an exposure time of 804 ms.

For Fig. 6, fluorescence signals excited with a 488-nm laser were visualized using a spinning-disk confocal system (CSU-X1; Yokogawa, Tokyo, Japan) mounted on an inverted microscope (IX71; Olympus, Tokyo, Japan) equipped with a 100×, 1.40 N.A. objective (UPLSAPO; Olympus). For about 6 min, including the entire process of spindle elongation at the 1-cell-stage embryo, digital images were acquired every 2 s with an EM-CCD camera (iXon; Andor Technology, Belfast, UK) controlled by Metamorph software (version 7.7.10.0) with an exposure time of 30 ms.

8.3. *S. mirabilis* sample preparation

S. mirabilis embryos were deformed using a microchamber [13,52]. We made the microchamber of polydimethyl-siloxane (SILPOT 184, Toray, Japan) with a mold made by using SU-8 negative photoresist. The chambers were columns of height 60 μm. The bottoms of the chambers were ellipses, and the aspect ratio ranged from 1.0 to 8.0. Also, the diameters of the bottom ranged from 138 μm to 153 μm in six stages. Embryos packed in the chamber were visualized by using a microscope (BX51; Olympus) equipped with a 20 × objective (UPLANFLN, Olympus). From the end of fertilization to the end of the first division, digital images were acquired every 1 s with a CCD camera (ORCA-ER C4742-80- 12AG, Hamamatsu Photonics KK, Shizuoka, Japan) controlled by IP Lab software (BD Biosciences, San Jose, CA).

Funding

This project was supported by JSPS KAKENHI (grant numbers JP15KT0083 to A.F. and A.K., and JP18H02414 to A.K.), by NIG-JOINT (77A2019) to A.F. and A.K., by the Naito Foundation to A.K., by the Sumitomo Foundation (141028) to A.K., and by Joint Support-Center for Data Science Research, ROIS to A.K.

CRedit authorship contribution statement

Shohei Tada: Writing – review & editing, Writing – original draft, Visualization, Validation, Software, Methodology, Investigation, Formal analysis, Data curation. **Yoshitaka Yamazaki:** Writing – review & editing, Writing – original draft, Visualization, Validation, Software, Methodology, Investigation, Formal analysis, Data curation. **Kazunori Yamamoto:** Writing – review & editing, Methodology, Investigation, Data curation. **Ken Fujii:** Writing – review & editing, Methodology, Investigation, Data curation. **Takahiro G. Yamada:** Writing – review & editing. **Noriko F. Hiroi:** Writing – review & editing, Methodology. **Akatsuki Kimura:** Writing – review & editing, Supervision, Resources, Project administration, Funding acquisition, Formal analysis, Conceptualization. **Akira Funahashi:** Writing – review & editing, Visualization, Supervision, Software, Resources, Project administration, Funding acquisition, Conceptualization.

Declaration of competing interest

The authors declare that they have no known competing financial interests or personal relationships that could have appeared to influence the work reported in this paper.

Data availability

The datasets generated and/or analyzed during the current study are available in the github repository, <https://github.com/funlab/MTSim>. The custom analysis codes created in this study are freely available through github (<https://github.com/funlab/MTSim>).

Acknowledgements

We thank Dr. Nicolas Minc for teaching A.K. the methods to change the shape of sea urchin zygotes using microchambers. We also thank Dr. Yohei Kikuchi for his advice on sea urchin experiments, Ms. Kazuko Oishi and Tomoko Ozawa for technical assistance, Dr. Yuki Hara for discussion, Dr. Shogo Kato for advice on angular statistics, and Drs. Genta Ueno and Shinya Nakano for advice on statistical methods. Some strains were provided by the *Caenorhabditis* Genetics Center, which is funded by the NIH Office of Research Infrastructure Programs (P40 OD010440).

Appendix A. Supplementary material

Supplementary material related to this article can be found online at <https://doi.org/10.1016/j.heliyon.2024.e25494>.

References

- [1] Jonathan M. Scholey, Ingrid Brust-Mascher, Alex Mogilner, Cell division, *Nature* 422 (2003) 746–752.
- [2] Yinan Liu, Douglas Robinson, Recent advances in cytokinesis: understanding the molecular underpinnings, *F1000Res.* 7 (1849) (2018) 10.
- [3] Sigrid Reinsch, Pierre Gönczy, Mechanisms of nuclear positioning, *J. Cell Sci.* (ISSN 0021-9533) 111 (16) (1998) 2283–2295, <https://doi.org/10.1242/jcs.111.16.2283>.
- [4] Edward L. Chambers, The movement of the egg nucleus in relation to the sperm aster in the Echinoderm egg, *J. Exp. Biol.* (ISSN 0022-0949) 16 (4) (1939) 409–424, <https://doi.org/10.1242/jeb.16.4.409>.
- [5] Miyako S. Hamaguchi, Yukio Hiramoto, Analysis of the role of astral rays in pronuclear migration in sand dollar eggs by the colcemid-UV method, *Dev. Growth Differ.* 28 (2) (1986) 143–156, <https://doi.org/10.1111/j.1440-169X.1986.00143.x>, <https://onlinelibrary.wiley.com/doi/abs/10.1111/j.1440-169X.1986.00143.x>.
- [6] Stephan Q. Schneider, Bruce Bowerman, Cell polarity and the cytoskeleton in the *Caenorhabditis elegans* zygote, *Annu. Rev. Genet.* 37 (1) (2003) 221–249, <https://doi.org/10.1146/annurev.genet.37.110801.142443>.
- [7] Tim Mitchison, Marc Kirschner, Dynamic instability of microtubule growth, *Nature* 312 (1984) 237–242.
- [8] Lisa R. Matthews, Philip Carter, Danielle Thierry-Mieg, Ken Kemphues, ZYG-9, a *Caenorhabditis elegans* protein required for microtubule organization and function, is a component of meiotic and mitotic spindle poles, *J. Cell Biol.* (ISSN 0021-9525) 141 (5) (1998) 1159–1168, <https://doi.org/10.1083/jcb.141.5.1159>.
- [9] Katayoun Afshar, Francis S. Willard, Kelly Colombo, Christopher A. Johnston, Christopher R. McCudden, David P. Siderovski, Pierre Gönczy, RIC-8 is required for GPR-1/2-dependent $G\alpha$ function during asymmetric division of *C. elegans* embryos, *Cell* (ISSN 0092-8674) 119 (2) (2004) 219–230, <https://doi.org/10.1016/j.cell.2004.09.026>.
- [10] Katayoun Afshar, Francis S. Willard, Kelly Colombo, David P. Siderovski, Pierre Gönczy, Cortical localization of the $G\alpha$ protein GPA-16 requires RIC-8 function during *C. elegans* asymmetric cell division, *Development* (ISSN 0950-1991) 132 (20) (2005) 4449–4459, <https://doi.org/10.1242/dev.02039>.
- [11] Stephan W. Grill, Jonathon Howard, Erik Schäffer, Ernst H.K. Stelzer, Anthony A. Hyman, The distribution of active force generators controls mitotic spindle position, *Science* 301 (5632) (2003) 518–521, <https://doi.org/10.1126/science.1086560>, <https://www.science.org/doi/abs/10.1126/science.1086560>.
- [12] Anthony A. Hyman, John G. White, Determination of cell division axes in the early embryogenesis of *Caenorhabditis elegans*, *J. Cell Biol.* (ISSN 0021-9525) 105 (5) (1987) 2123–2135, <https://doi.org/10.1083/jcb.105.5.2123>.
- [13] Nicolas Minc, David Burgess, Fred Chang, Influence of cell geometry on division-plane positioning, *Cell* (ISSN 0092-8674) 144 (3) (2011) 414–426, <https://doi.org/10.1016/j.cell.2011.01.016>.
- [14] Martin Wühr, Edwin S. Tan, Sandra K. Parker, H. William Detrich, Timothy J. Mitchison, A model for cleavage plane determination in early amphibian and fish embryos, *Curr. Biol.* (ISSN 0960-9822) 20 (22) (2010) 2040–2045, <https://doi.org/10.1016/j.cub.2010.10.024>.
- [15] Akatsuki Kimura, Shuichi Onami, Computer simulations and image processing reveal length-dependent pulling force as the primary mechanism for *C. elegans* male pronuclear migration, *Dev. Cell* (ISSN 1534-5807) 8 (5) (2005) 765–775, <https://doi.org/10.1016/j.devcel.2005.03.007>.
- [16] Kenji Kimura, Akatsuki Kimura, A novel mechanism of microtubule length-dependent force to pull centrosomes toward the cell center, *BioArchitecture* 1 (2) (2011) 74–79, <https://doi.org/10.4161/bioa.1.2.15549>.
- [17] Akatsuki Kimura, Shuichi Onami, Chapter 23 - Modeling microtubule-mediated forces and centrosome positioning in *Caenorhabditis elegans* embryos, in: Lynne Cassimeris, Phong Tran (Eds.), *Microtubules: in Vivo*, in: *Methods in Cell Biology*, vol. 97, Academic Press, 2010, pp. 437–453.
- [18] Hirokazu Tanimoto, Akatsuki Kimura, Nicolas Minc, Shape-motion relationships of centering microtubule asters, *J. Cell Biol.* (ISSN 0021-9525) 212 (7) (2016) 777–787, <https://doi.org/10.1083/jcb.201510064>.
- [19] Carlos Garzon-Coral, Horatiu A. Fantana, Jonathon Howard, A force-generating machinery maintains the spindle at the cell center during mitosis, *Science* 352 (6289) (2016) 1124–1127, <https://doi.org/10.1126/science.aad9745>, <https://www.science.org/doi/abs/10.1126/science.aad9745>.
- [20] Johnathan L. Meaders, Salvador N. de Matos, David R. Burgess, A pushing mechanism for microtubule aster positioning in a large cell type, *Cell Rep.* (ISSN 2211-1247) 33 (1) (2020) 108213, <https://doi.org/10.1016/j.celrep.2020.108213>.
- [21] Ana Joaquina Jimenez, Alexandre Schaeffer, Chiara De Pascalis, Gaëlle Letort, Benoit Vianay, Michel Bornens, Matthieu Piel, Laurent Blanchoin, Manuel Théry, Acto-myosin network geometry defines centrosome position, *Curr. Biol.* (ISSN 0960-9822) 31 (6) (2021) 1206–1220.e5, <https://doi.org/10.1016/j.cub.2021.01.002>.
- [22] Yuki Hara, Akatsuki Kimura, Cell-size-dependent spindle elongation in the *Caenorhabditis elegans* early embryo, *Curr. Biol.* (ISSN 0960-9822) 19 (18) (2009) 1549–1554, <https://doi.org/10.1016/j.cub.2009.07.050>.
- [23] Cleopatra Kozłowski, Martin Srayko, Francois Nedelec, Cortical microtubule contacts position the spindle in *C. elegans* embryos, *Cell* (ISSN 0092-8674) 129 (3) (2007) 499–510, <https://doi.org/10.1016/j.cell.2007.03.027>.
- [24] Akatsuki Kimura, Shuichi Onami, Local cortical pulling-force repression switches centrosomal centration and posterior displacement in *C. elegans*, *J. Cell Biol.* (ISSN 0021-9525) 179 (7) (2007) 1347–1354, <https://doi.org/10.1083/jcb.200706005>.
- [25] Steven H. Strogatz, *Nonlinear Dynamics and Chaos: with Applications to Physics, Biology, Chemistry, and Engineering*, CRC Press, 2018.
- [26] Reza Farhadifar, Che-Hang Yu, Gunar Fabig, Hai-Yin Wu, David B. Stein, Matthew Rockman, Thomas Müller-Reichert, Michael J. Shelley, Daniel J. Needleman, Stoichiometric interactions explain spindle dynamics and scaling across 100 million years of nematode evolution, *eLife* (ISSN 2050-084X) 9 (sep 2020) e55877, <https://doi.org/10.7554/eLife.55877>.
- [27] Stephan W. Grill, Anthony A. Hyman, Spindle positioning by cortical pulling forces, *Dev. Cell* 8 (4) (2005) 461–465.
- [28] Hai-Yin Wu, Gökberk Kabacaoglu, Ehssan Nazockdast, Huan-Cheng Chang, Michael J. Shelley, Daniel J. Needleman, Laser ablation and fluid flows reveal the mechanism behind spindle and centrosome positioning, *Nat. Phys.* (2023), <https://doi.org/10.1038/s41567-023-02223-z>.
- [29] Kazunori Yamamoto, Akatsuki Kimura, An asymmetric attraction model for the diversity and robustness of cell arrangement in nematodes, *Development* (ISSN 0950-1991) 144 (23) (2017) 4437–4449, <https://doi.org/10.1242/dev.154609>.

- [30] Victoria E. Foe, George von Dassow, Stable and dynamic microtubules coordinately shape the myosin activation zone during cytokinetic furrow formation, *J. Cell Biol.* (ISSN 0021-9525) 183 (3) (2008) 457–470, <https://doi.org/10.1083/jcb.200807128>.
- [31] Gregory C. Rogers, Kitty K. Chui, Edwin W. Lee, Karen P. Wedaman, David J. Sharp, Gina Holland, Robert L. Morris, Jonathan M. Scholey, A Kinesin-related protein, Krp180, positions prometaphase spindle poles during early sea urchin embryonic cell division, *J. Cell Biol.* (ISSN 0021-9525) 150 (3) (2000) 499–512, <https://doi.org/10.1083/jcb.150.3.499>.
- [32] Dae Hwi Park, Lesilee S. Rose, Dynamic localization of LIN-5 and GPR-1/2 to cortical force generation domains during spindle positioning, *Dev. Biol.* (ISSN 0012-1606) 315 (1) (2008) 42–54, <https://doi.org/10.1016/j.ydbio.2007.11.037>.
- [33] Sylvie Bussion, Denis Dujardin, Anne Moreau, Jim Dompierre, Jan R. De Mey, Dynein and dynactin are localized to astral microtubules and at cortical sites in mitotic epithelial cells, *Curr. Biol.* (ISSN 0960-9822) 8 (9) (1998) 541–544, [https://doi.org/10.1016/S0960-9822\(98\)70208-8](https://doi.org/10.1016/S0960-9822(98)70208-8).
- [34] Marileen Dogterom, Jacob W.J. Kerssemakers, Guillaume Romet-Lemonne, Marcel E. Janson, Force generation by dynamic microtubules, *Curr. Opin. Cell Biol.* (ISSN 0955-0674) 17 (1) (2005) 67–74, <https://doi.org/10.1016/j.ccb.2004.12.011>.
- [35] P.T. Tran, L. Marsh, V. Doye, S. Inoué, F. Chang, A mechanism for nuclear positioning in fission yeast based on microtubule pushing, *J. Cell Biol.* (ISSN 0021-9525) 153 (2) (2001) 397–412, <https://doi.org/10.1083/jcb.153.2.397>.
- [36] Ingrid Brust-Mascher, Jonathan M. Scholey, Microtubule flux and sliding in mitotic spindles of *Drosophila* embryos, *Mol. Biol. Cell* 13 (11) (2002) 3967–3975, <https://doi.org/10.1091/mbc.02-05-0069>.
- [37] Stephan W. Grill, Pierre Goënczy, Ernst HK Stelzer, Anthony A. Hyman, Polarity controls forces governing asymmetric spindle positioning in the *Caenorhabditis elegans* embryo, *Nature* 409 (2001) 630–633.
- [38] George von Dassow, Koen J.C. Verbrugghe, Ann L. Miller, Jenny R. Sider, William M. Bement, Action at a distance during cytokinesis, *J. Cell Biol.* (ISSN 0021-9525) 187 (6) (2009) 831–845, <https://doi.org/10.1083/jcb.200907090>.
- [39] Yukio Hiramoto, Yoshitaro Nakano, Micromanipulation studies of the mitotic apparatus in sand dollar eggs, *Cell Motil.* 10 (1988) 172–184, <https://doi.org/10.1002/cm.970100122>, <https://onlinelibrary.wiley.com/doi/abs/10.1002/cm.970100122>.
- [40] Adam M. Saunders, James Powers, Susan Strome, William M. Saxton, Kinesin-5 acts as a brake in anaphase spindle elongation, *Curr. Biol.* (ISSN 0960-9822) 17 (12) (2007) R453–R454, <https://doi.org/10.1016/j.cub.2007.05.001>.
- [41] Sydney Brenner, The genetics of *Caenorhabditis elegans*, *Genetics* (ISSN 1943-2631) 77 (1) (1974) 71–94, <https://doi.org/10.1093/genetics/77.1.71>.
- [42] Ravi S. Kamath, Maruxa Martínez-Campos, Peder Zipperlen, Andrew G. Fraser, Julie Ahringer, Effectiveness of specific RNA-mediated interference through ingested double-stranded RNA in *Caenorhabditis elegans*, *Genome Biol.* 2 (research0002-1) (2000).
- [43] Andrew G. Fraser, Ravi S. Kamath, Peder Zipperlen, Maruxa Martínez-Campos, Marc Sohrmann, Julie Ahringer, Functional genomic analysis of *C. elegans* chromosome I by systematic RNA interference, *Nature* 408 (2000) 325–330.
- [44] E.M. Purcell, Life at low Reynolds number, *Am. J. Phys.* 45 (1) (1977) 3–11, <https://doi.org/10.1119/1.10903>.
- [45] Kazuhisa Kinoshita, Bianca Habermann, Anthony A. Hyman, XMAP215: a key component of the dynamic microtubule cytoskeleton, *Trends Cell Biol.* (ISSN 0962-8924) 12 (6) (2002) 267–273, [https://doi.org/10.1016/S0962-8924\(02\)02295-X](https://doi.org/10.1016/S0962-8924(02)02295-X).
- [46] Yukio Hiramoto, Rheological properties of sea urchin eggs, *Biorheology* 6 (3) (1970) 201–234.
- [47] Markus Decker, Steffen Jaensch, Andrei Pozniakovsky, Andrea Zinke, Kevin F. O'Connell, Wolfgang Zachariae, Eugene Myers, Anthony A. Hyman, Limiting amounts of centrosome material set centrosome size in *C. elegans* embryos, *Curr. Biol.* (ISSN 0960-9822) 21 (15) (2011) 1259–1267, <https://doi.org/10.1016/j.cub.2011.06.002>.
- [48] D. Sage, F.R. Neumann, F. Hediger, S.M. Gasser, M. Unser, Automatic tracking of individual fluorescence particles: application to the study of chromosome dynamics, *IEEE Trans. Image Process.* 14 (9) (2005) 1372–1383, <https://doi.org/10.1109/TIP.2005.852787>.
- [49] Akatsuki Kimura, Antonio Celani, Hiromichi Nagao, Timothy Stasevich, Kazuyuki Nakamura, Estimating cellular parameters through optimization procedures: elementary principles and applications, *Front. Physiol.* (ISSN 1664-042X) 6 (2015), <https://doi.org/10.3389/fphys.2015.00060>, <https://www.frontiersin.org/articles/10.3389/fphys.2015.00060>.
- [50] Aiya K. Yesbolatova, Ritsuko Arai, Takahiro Sakae, Akatsuki Kimura, Formulation of chromatin mobility as a function of nuclear size during *C. elegans* embryogenesis using polymer physics theories, *Phys. Rev. Lett.* 128 (Apr 2022) 178101, <https://doi.org/10.1103/PhysRevLett.128.178101>, <https://link.aps.org/doi/10.1103/PhysRevLett.128.178101>.
- [51] Johannes Schindelin, Ignacio Arganda-Carreras, Erwin Frise, Verena Kaynig, Mark Longair, Tobias Pietzsch, Stephan Preibisch, Curtis Rueden, Stephan Saalfeld, Benjamin Schmid, et al., Fiji: an open-source platform for biological-image analysis, *Nat. Methods* 9 (2012) 676–682.
- [52] Fred Chang, Erdinc Atilgan, David Burgess, Nicolas Minc, Manipulating cell shape by placing cells into micro-fabricated chambers, in: D. Sharp (Ed.), *Methods in Molecular Biology (Methods and Protocols)*, in: *Mitosis*, vol. 1136, Humana Press, 2014, pp. 281–290.
- [53] Steven P. Gross, Michael A. Welte, Steven M. Block, Eric F. Wieschaus, Dynein-mediated Cargo transport in vivo: a switch controls travel distance, *J. Cell Biol.* (ISSN 0021-9525) 148 (5) (2000) 945–956, <https://doi.org/10.1083/jcb.148.5.945>.
- [54] Jonathon Howard, *Mechanics of Motor Proteins and the Cytoskeleton*, Sinauer Associates, ISBN 9780878933334, 2001, <https://books.google.co.jp/books?id=-mmnQgAACAAJ>.
- [55] François Nédélec, Computer simulations reveal motor properties generating stable antiparallel microtubule interactions, *J. Cell Biol.* (ISSN 0021-9525) 158 (6) (2002) 1005–1015, <https://doi.org/10.1083/jcb.200202051>.
- [56] Lynne Cassimeris, Nancy K. Pryer, Edward D. Salmon, Real-time observations of microtubule dynamic instability in living cells, *J. Cell Biol.* (ISSN 0021-9525) 107 (6) (1988) 2223–2231, <https://doi.org/10.1083/jcb.107.6.2223>.
- [57] Lisa D. Belmont, Anthony A. Hyman, Kenneth E. Sawin, Timothy J. Mitchison, Real-time visualization of cell cycle-dependent changes in microtubule dynamics in cytoplasmic extracts, *Cell* (ISSN 0092-8674) 62 (3) (1990) 579–589, [https://doi.org/10.1016/0092-8674\(90\)90022-7](https://doi.org/10.1016/0092-8674(90)90022-7).
- [58] Fulvia Verde, Marileen Dogterom, Ernst Stelzer, Eric Karsenti, Stanislas Leibler, Control of microtubule dynamics and length by cyclin A- and cyclin B-dependent kinases in *Xenopus* egg extracts, *J. Cell Biol.* (ISSN 0021-9525) 118 (5) (1992) 1097–1108, <https://doi.org/10.1083/jcb.118.5.1097>.
- [59] Rama Dhamodharan, Patricia Wadsworth, Modulation of microtubule dynamic instability in vivo by brain microtubule associated proteins, *J. Cell Sci.* (ISSN 0021-9533) 108 (4) (1995) 1679–1689, <https://doi.org/10.1242/jcs.108.4.1679>.
- [60] Frederick Gittes, Brian Mickey, Jilda Nettleton, Jonathon Howard, Flexural rigidity of microtubules and actin filaments measured from thermal fluctuations in shape, *J. Cell Biol.* (ISSN 0021-9525) 120 (4) (1993) 923–934, <https://doi.org/10.1083/jcb.120.4.923>.
- [61] Roop Mallik, Brian C. Carter, Stephanie A. Lex, Stephen J. King, Steven P. Gross, Cytoplasmic dynein functions as a gear in response to load, *Nature* 427 (2004) 649–652.